CrystEngComm

Accepted Manuscript

This article can be cited before page numbers have been issued, to do this please use: I. S. Veljkovi, D. Ž. Veljkovi, G. G. Sari, I. M. Stankovic and S. D. Zaric, *CrystEngComm*, 2020, DOI: 10.1039/D0CE00211A.

ROYAL SOCIETY OF CHEMISTRY

rsc.li/crystengcomm

View Article Online
DOI: 10.1039/D0CE00211A

ARTICLE

What is the preferred geometry of sulfur − disulfide interactions?

Ivana S. Veljković,[a] Dušan Ž. Veljković,[b] Gordana G. Sarić,[b] Ivana M. Stanković,[a] Snežana D. Zarić*[b]

Received 00th January 20xx,
Accepted 00th January 20xx

DOI: 10.1039/x0xx00000x

Non-covalent interactions between disulfide fragment and sulfur atom were studied in crystal structures of small molecules and by quantum chemical calculations. Statistical analysis of geometrical data from Cambridge Structural Database (CSD) reveals that in most cases interactions between sulfur and disulfide bond are bifurcated. Quantum chemical calculations are in agreement with those findings. The strong interaction energy was calculated for bifurcated interaction ($E_{CCSD(T)/CBS}$ = -2.83 kcal/mol) considering the region along disulfide bond. Non-bifurcated interactions are weaker except in cases where σ-*hole* interaction is possible or in cases where S···S interaction is accompanied by additional hydrogen bonds ($E_{CCSD(T)/CBS}$ = -3.26 kcal/mol). SAPT decomposition analysis shows that dispersion is the main attractive force in studied systems while electrostatics play crucial role in defining geometry of interactions.

Introduction

Attractive interactions between a divalent sulfur and adjacent heteroatom were recognized decades ago in the crystals of small organic compounds.[1-4] In these crystal structures, short S···X (X = O, N, S) contacts were found.[2] It was shown that X atom involved in these interactions was mainly located in the backside of one of the two covalent bonds.[3-5] Interactions between homoatomic chalcogen centers (O, S, Se, Te) were studied by quantum chemical calculations.[6,7] Results showed that the strength of the interaction increases from oxygen to tellurium, but in all studied model systems weak hydrogen bonds occur along with the chalcogen-chalcogen interactions.[7] S···X interactions are also present in the proteins.[8-12] Although weak, these interactions play a prominent role in both stabilization of the three-dimensional structure of proteins and in the protein function.[8]

One of the most studied types of S···X interactions are S···S interactions.[13-18] These contacts are found in many important chemical and biochemical systems like small organic molecules and proteins. Intermolecular S···S interactions are also recognized in the structures of some well-known organic semiconductors.[19-23] Numerous studies have pointed out the importance of S···S interactions for the structure, function[19,20] and supramolecular assembly of these molecules.[21,22,23] S···S interactions are also well-known in organometallic and coordination compounds.[17b-e]

The early studies showed that nonbonded S···S interactions in organic crystals may be stabilized by the orbital interaction[1,3,4] of sulfur atoms. Similar orbital interaction have been found in protein structures; S–S···S–S chalcogen bond has linear S–S···S or C–S···S alignment.[12] S···S interactions were also studied in the crystal structure of L-Cystine.[24] Energy of S···S interaction between two molecules of L-cystine in experimental L-cystine crystal structure was predicted by PBE-MBD method to be -3.46 kcal/mol.

Distances between two interacting atoms can sometimes be shorter than the sum of the van der Waals radii.[5,13] These close distances may be explained by *σ-hole* concept.[15,25-27] Model system containing methanethiol dimer in non-parallel orientation with possible *σ-hole* interaction was studied by quantum chemical calculations. Results of calculations showed that in this model system S···S interaction is the strongest, -2.20 kcal/mol.[16] Statistical analysis of crystallographic data archived in Cambridge Structural Database (CSD)[28] showed that preferred orientation between cysteine residues is a parallel orientation.[16] Based on the parallel geometries found in CSD, model systems for quantum chemical calculations of interaction energies between these molecules were made. The strongest CCSD(T)/CBS interaction energy in these model systems was calculated to be -1.80 kcal/mol.

Recent crystallographic and computational study reveals that C=S···S=C interactions are very common in crystal structures of small organic molecules.[17] Results of quantum chemical calculations at CCSD(T)/CBS level performed on $(X_2CS)_2$ dimers (X = H, NH_2, OH, F, Cl) shows that interactions in these systems are attractive. The weakest interaction was recognized in $(H_2CS)_2$ dimer and it was calculated to be -0.66 kcal/mol, while the strongest interaction was found in $(Cl_2CS)_2$ dimer and the energy was calculated to be -1.07 kcal/mol.

Geometries and energies of interactions between disulfide fragments and various atoms and ions were also studied in crystal structures and by quantum chemical calculations.[10,12,29]

[a] Institute of Chemistry, Technology and Metallurgy, University of Belgrade, Njegoševa 12, 11000 Belgrade, Serbia.
[b] University of Belgrade - Faculty of Chemistry, Studentski trg 12-16, 11000, Belgrade, Serbia.

† Footnotes relating to the title and/or authors should appear here.
Electronic Supplementary Information (ESI) available: [details of any supplementary information available should be included here]. See DOI: 10.1039/x0xx00000x

View Article Online
DOI: 10.1039/D0CE00211A

The strongest linear S-S···O interaction was found in model system consisting of $CH_3CONHCH_3$ and CH_3SSCH_3. Interaction energy calculated at the MP2/6-31G(d) level for this model system is -3.21 kcal/mol.[10]

Non−linear interactions in which one atom simultaneously interacts with two other atoms are called bifurcated interactions. Many weak non−covalent contacts can exist in form of bifurcated interactions.[29-33] Combined crystallographic and quantum chemical studies showed that in case of aromatic C−H donors bifurcated C−H/O interactions are stronger than linear ones. Energies calculated at MP2/cc-pVTZ level in benzene/water model systems for bifurcated C−H/O interactions are estimated to be -1.38 kcal/mol, while for linear C−H/O interactions are -1.28 kcal/mol.[30] Interactions involving special cases of identical moieties of sulfur and selenium trichalconides (containing S_3 or Se_3 bridge) are mostly bifurcated.[34] Depending on the conformation of substituents, bifurcated or double chalcogen bonding patterns could be found in crystal structures of sulfur and selenium trichalconide fragments.[34]

Energies of non−linear interactions between S−S fragment and nitrogen and oxygen atoms from NH_3 and H_2O molecules were also calculated. The interaction energies of the bifurcated S−S···Y (Y = N, O) chalcogen interactions between 1,2,4-dithiazolidine-3,5-dione (DtsNH) and NH_3 and H_2O molecules were calculated using MP2/aug-cc-pVDZ level of theory; the interactions are quite strong: -4.56 and -3.52 kcal/mol, respectively.[29]

Although geometries of interactions between S−S fragments and various atoms like O and N were studied, there are no systematic studies related to the geometries and energies of S−S···S interactions. Here we studied geometries and energies of S−S···S interactions using quantum chemical calculations and statistical analysis of crystallographic data from CSD. The main goal of this work was to combine experimental data from crystal structures with high level quantum chemical calculations to determine whether these interactions are predominantly bifurcated or non-bifurcated. To the best of our knowledge, this is the first systematic study of geometries and energies of S−S···S interactions.

Methodology

CSD Search

The search of Cambridge Structural Database (CSD, version 5.39, November 2018)[28] was performed using the ConQuest 1.20 program.[35] All the structures containing contacts between sulfur and disulfide bond and satisfying certain geometrical criteria were extracted. The geometrical parameters used to search CSD and to characterize these interactions are displayed in Figure 1. The contact was considered S−S···S interaction if at least one distance between sulfur atoms *d* is shorter than 5.0 Å. Interacting sulfur atom from disulfide bond (S_1) is the one which is at the shorter distance from sulfur atom (labeled as S_3) of another molecule.

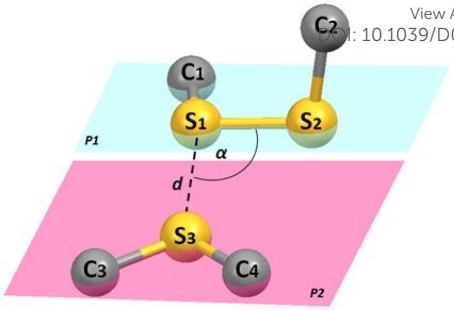

Figure 1. Geometrical parameters used to describe interactions between sulfur and disulfide bond: d is the distance between two interacting sulfur atoms while α is the angle formed by S_2-S_1-S_3 atoms and contains shorter distance d. Planes P_1 and P_2 contain C_1-S_1-S_2 and C_3-S_3-C_4 atoms, respectively.

There were no restrictions in respect to the nature of substituents attached to atoms C_1 and C_2; structures with all types of substituents were taken into consideration for further analysis.

Quantum Chemical Calculations

Model system consisting of dimethyl sulfide and dimethyl disulfide was used for the calculations of S−S···S interaction energies. Using the Gaussian 09 program package[36], geometries of isolated dimethyl sulfide and dimethyl disulfide were optimized at the MP2/cc-pVTZ[37,38] level and confirmed as true minimum by performing the calculations of vibrational frequencies (Tables S1 and S2, Supporting Information). Potential energy surface was calculated at the MP2/cc-pVQZ level of theory[37,39] since it was shown that energies of S···S interactions calculated using this level of theory are in excellent agreement with the energies calculated using CCSD(T)/CBS method.[16,40] For most stable orientations of two interacting molecules CCSD(T)/CBS interaction energies were also calculated by applying the extrapolation scheme proposed by Mackie and DiLabio.[41] Calculated energies were corrected for basis set superposition error (BSSE) using the Counterpoise method.[42]

Energy decomposition analysis of the strongest interaction energy was performed using SAPT 2+3 method,[43,44] and aug-cc-PVTZ basis set.[39] SAPT analysis was performed using the Psi4 program package.[45] This method calculates the overall interaction energy as a sum of electrostatic, dispersion, exchange and induction energies. Electrostatic potential of dimethyl sulfide and dimethyl disulfide molecules were mapped from its MP2/cc-pVTZ wave function file on the 0.001 a.u. density surface,[46] using the Wave Function Analysis-Surface Analysis Suite (WFA-SAS) program.[47]

Results and discussion

Analysis of the CSD crystal structures

Crystal structures obtained by CSD search were studied by analysing geometrical parameters to determine geometrical characteristics of S−S···S interactions. CSD was searched using

the criteria described in Methodology section. The CSD search derived 216 structures with 667 S–S···S contacts which are further analysed.

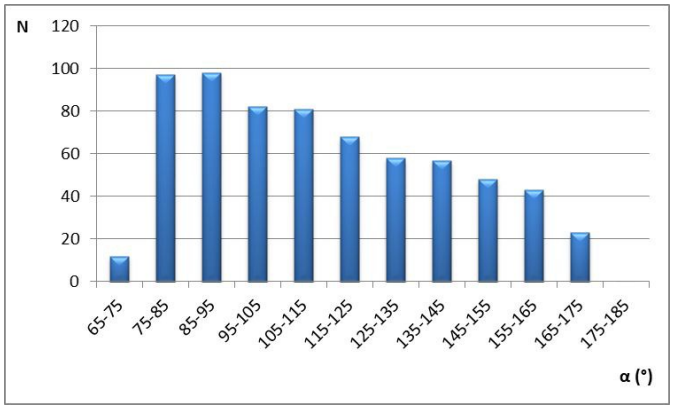

Figure 2. The distribution of angle between disulfide bond and atom S3 (angle α) for contacts with shortest distance *d* (Figure 1)

In order to investigate geometry of S–S···S interactions within the given fragment (Figure 1), a statistical analysis of distance *d* and angle *α* has been performed. Distribution of distance *d* values shows that most frequent S···S distances in these structures are in the interval 3.6-4.0 Å (Figure S1). Distribution of angle *α* values is given in Figure 2 and shows slight preference for contacts with angle *α* values in the range from 75° to 95° that mostly corresponds to bifurcated interaction. Interactions with angle *α* values above 90° are very common in studied structures; however, these values do not correspond to the bifurcated interactions. Large number of these structures could be consequence of the formation of hydrogen bonds between interacting sulfur atoms and hydrogen atoms attached to C_1 and C_2 substituents. Interactions with an angle *α* below 65°, as well as in the interval from 175° to 180°, were not observed in crystals.

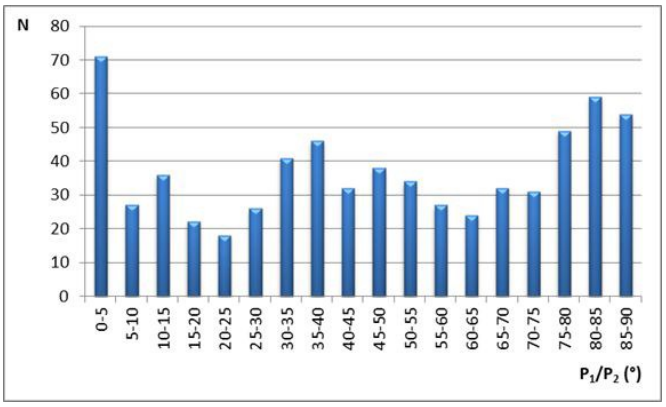

Figure 3. The distribution of angle P_1/P_2 formed between plains (Figure 1) in which interacting molecules are positioned.

Angle formed between planes P_1 and P_2 (Figure 1) was also analyzed in crystal structures (Figure 3). The most frequent contacts with P_1/P_2 angle are in the range from 0° to 5°. However, all other angles are also present, while there is a slight preference for angles in the range 75-90°. When considering the positions of sulfur interacting with the disulfide bond, we visualized the spatial distribution of the disulfide/sulfur interactions geometry (Figure S2). The distribution indicates that in majority of crystal structures sulfur atoms are located in the region of S-S bond (Figure S2 B).

View Article Online
DOI: 10.1039/C6CE00311A

Energies of interaction

Potential energy surfaces were calculated at MP2/cc-pVQZ level using model systems containing dimethyl disulfide and dimethyl sulfide molecules in different orientations. Model systems were based on the geometries with P_1/P_2 angle of 0.0° and 90.0°, since these are two extreme angles, and significant number of contacts in the crystal structures has these angles (Figure 3). We made four model systems A, B, C and D presented in Figure 4.

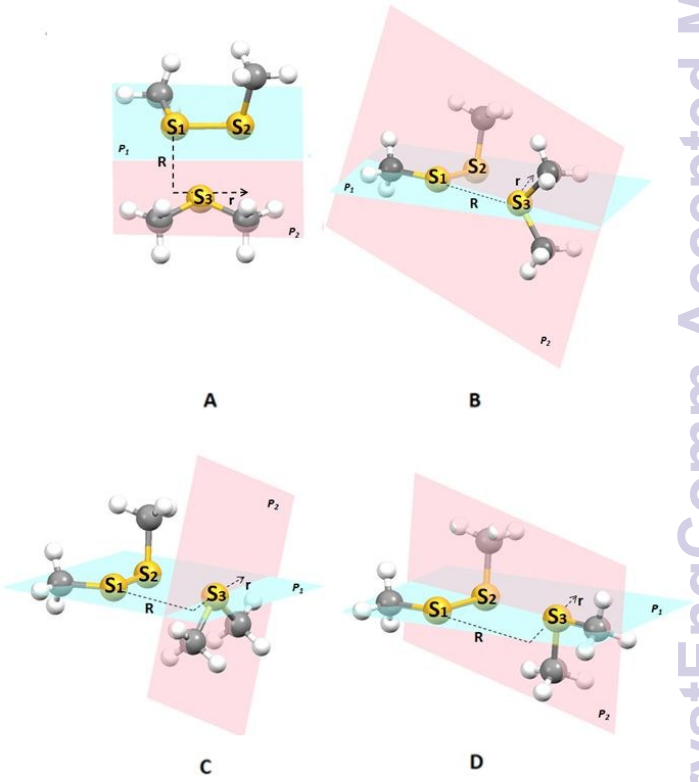

Figure 4. Model systems used for the calculations of S–S···S interaction energies. *R* is the normal distance, while *r* represents horizontal displacement (offset).

To evaluate S–S···S interaction energy, for each of the model systems, we have examined the entire area around the disulfide bond that was divided into three regions as shown in Figure 5. In all calculations the geometries of dimethyl

disulfide and dimethyl sulfide were fixed, while they were moved to calculate potential energy surface.

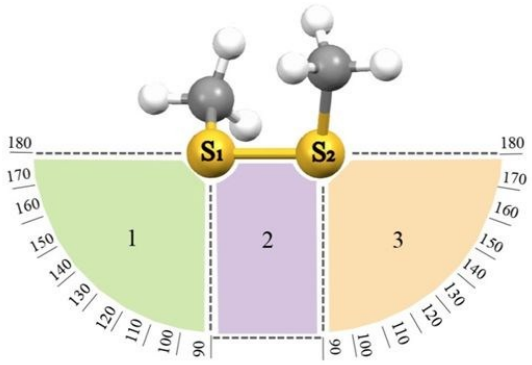

Figure 5. Area around disulfide bond is divided into three regions. First (green color) is the region around the sulfur atom labeled as S_1, second (violet color) represents the region along S_1–S_2 bond while third (orange color) represents the region around the sulfur atom labeled as S_2.

Within the region of disulfide bond (region 2, Figure 5), in all model systems the position of dimethyl disulfide was fixed, while the position of another molecule is systematically changed by increasing the value of offset *r* (Figure 4). For each offset value *r* the optimal distance *R* between molecules was determined. The starting position was the one with α angle of 90° (Figure 1) in the C–S–S plane (non-bifurcated S_2–S_1···S_3 interaction). The displacement of dimethyl sulfide was done along the disulfide bond (S–S distance is 2.045 Å), forming bifurcated bonds and finally a second non-bifurcated interaction (S_1–S_2···S_3) is formed. To investigate interactions in regions around S_1 and S_2 atoms (regions 1 and 3, Figure 5) the dimethyl disulfide was fixed and position of dimethyl sulfide was changed by increasing the S_2–S_1···S_3 or S_1–S_2···S_3 angle by 10° while simultaneously changing the S_1···S_3 or S_2···S_3 distance, respectively.

View Article Online DOI: 10.1039/D0CE00211A

For model system **A**, at an offset value of 0.0 Å, (**A_{NB1}**, Figure 6), the calculated MP2/cc-pVQZ interaction energy is -1.22 kcal/mol. CCSD(T)/CBS interaction energy of the same interaction is -1.20 kcal/mol. As in all the other model systems, interaction energy calculated at MP2/cc-pVQZ level was in excellent agreement with interaction energies calculated at CCSD(T)/CBS level (Table S3).

The strongest S–S···S interaction energy in region 2 (Figure 5) for model system **A** was calculated for bifurcated **A_B** geometry (Figure 6) at r = 0.6 Å with CCSD(T)/CBS interaction energy of -1.54 kcal/mol. This bifurcated S–S···S interaction energy is only 0.26 kcal/mol weaker than previously calculated strongest S···S interaction (-1.80 kcal/mol) in parallel orientation of two methanetiol molecules and 0.66 kcal/mol weaker in respect to the strongest calculated S···S interaction in electrostatically favored dimer of methanethiol molecules (-2.20 kcal/mol).[16] The value of S_2–S_1···S_3 angle in **A_B** geometry (Figure 6) is 79.99° while S_1···S_3 distance is 3.45 Å (shorter than the sum of their van der Waals radii, 3.60 Å)[48,49] and S_2···S_3 distance is 3.69 Å.

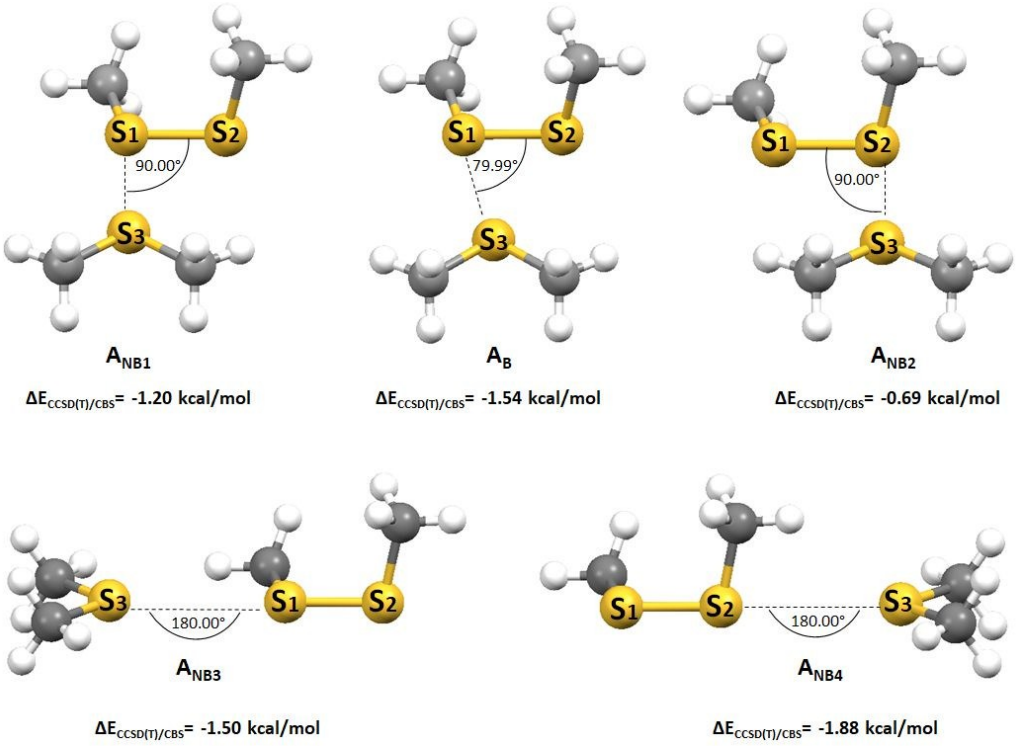

Figure 6. Geometries and energies of four non-bifurcated (A_{NB1}, A_{NB2}, A_{NB3} and A_{NB4}) and one bifurcated (A_B) interactions for model system A. Planes defined with atoms C–S_1–S_2 and C–S_3–C atoms are coplanar.

View Article Online
DOI: 10.1039/D0CE00211A

Similar $S_1\cdots S_3$ and $S_2\cdots S_3$ distances for both interactions correspond to the bifurcated S–S···S interaction. This result is in agreement with the data obtained from the crystal structures since a significant number of S–S···S contacts have a value of $S_2–S_1\cdots S_3$ angle in the range from 75° to 95° (Figure 2). With the additional increase of the offset value, the attractive S–S···S interactions become weaker (Figure S3, Supporting Information). In the case when S_3 atom is oriented towards the S_2 atom (**A_{NB2}** geometry, Figure 6), the interaction energy calculated at CCSD(T)/CBS level is only -0.69 kcal/mol. The $S_2\cdots S_3$ distance in this geometry is 3.90 Å while $S_2–S_1\cdots S_3$ angle is 62.33°.

In regions 2 and 3, around S_1 and S_2 atoms, the calculated interactions are stronger; in the geometry **A_{NB3}** with $S_2–S_1\cdots S_3$ angle of 180°, CCSD(T)/CBS interaction energy is -1.50 kcal/mol, while in the geometry **A_{NB4}** with $S_1–S_2\cdots S_3$ angle of 180°, CCSD(T)/CBS interaction energy is -1.88 kcal/mol, (Figure 6 and Table S4, Supporting Information).

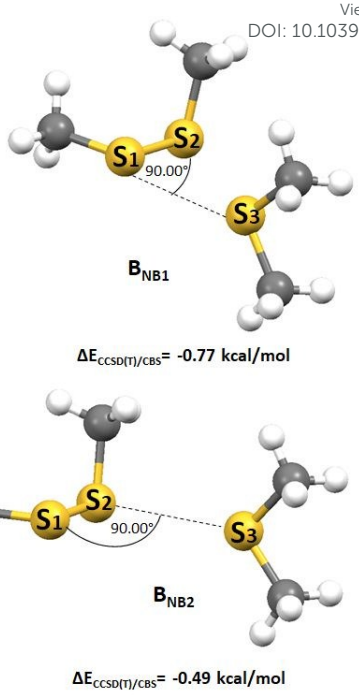

Figure 7. Geometries and energies of two non-bifurcated (B_{NB1} and B_{NB2}) interactions for model system B. Planes defined with atoms C–S_1–S_2 and C–S_3–C atoms are normal.

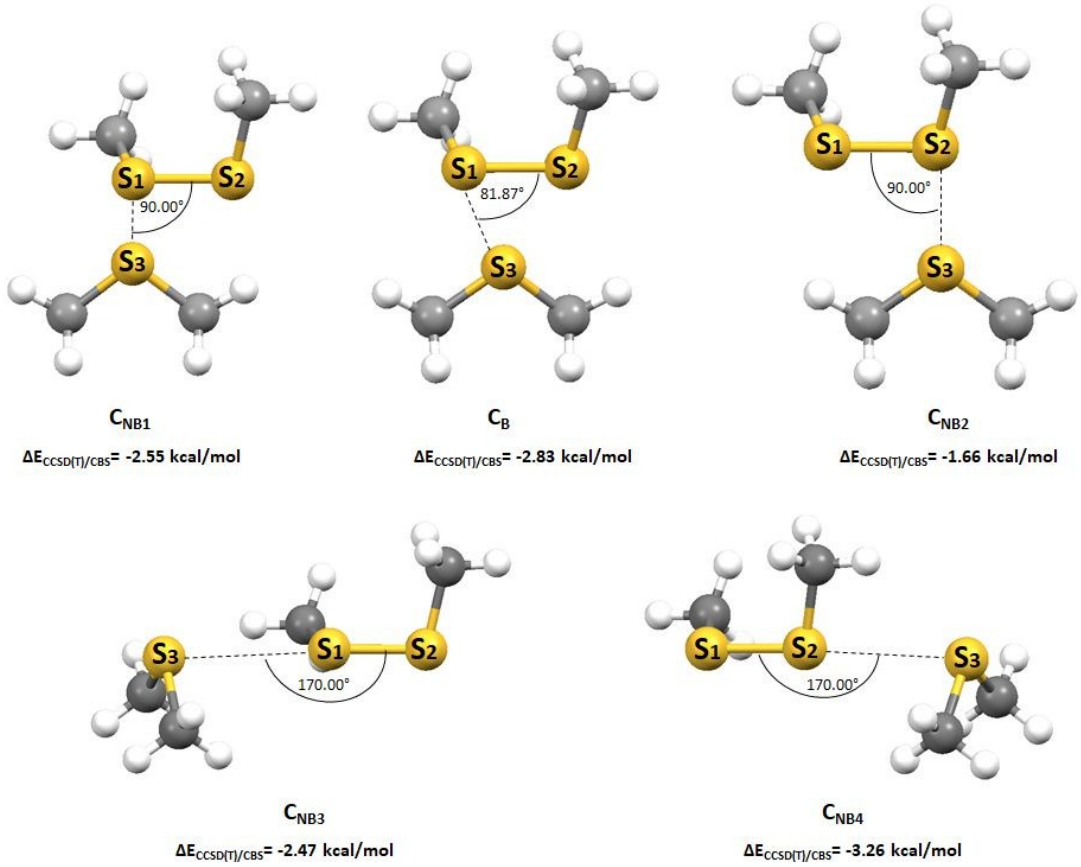

Figure 8. Geometries and energies of four non-bifurcated (C_{NB1}, C_{NB2}, C_{NB3} and C_{NB4}) and one bifurcated (C_B) interactions for model system C. Planes defined with atoms C–S_1–S_2 and C–S_3–C atoms are orthogonal.

View Article Online
DOI: 10.1039/D0CE00211A

ARTICLE

For model system **B**, the interaction energy difference between two non-bifurcated $\mathbf{B_{NB1}}$ and $\mathbf{B_{NB2}}$ geometries is relatively small; $E_{CCSD(T)/CBS}$ = -0.77 kcal/mol and $E_{CCSD(T)/CBS}$ = -0.49 kcal/mol, respectively (Figure 7). It is worth mentioning that in this case, no minimum for bifurcated interaction was detected. With an increase in offset r, S–S···S interactions are weakening almost linearly (Figure S4, Supporting Information).

Interaction energies in all geometries in region 2 (Figure 5) of model system **B** are relatively weak due to repulsive interactions between methyl groups attached to sulfur atoms of interacting molecules. Furthermore, two possible geometries for model system **B** in regions 1 and 3 (Figure 5) are completely the same as corresponding geometries of model system **A**; geometry with S_2–S_1···S_3 angle (region around S_1 atom) is the same as $\mathbf{A_{NB4}}$ geometry ($E_{CCSD(T)/CBS}$ = -1.88 kcal/mol, Table S4) while geometry with S_1–S_2···S_3 angle (region around S_2 atom) is the same as $\mathbf{A_{NB3}}$ geometry ($E_{CCSD(T)/CBS}$ = -1.50 kcal/mol, Table S4).

In another normal orientation (model system **C**, Figure 4), bifurcated interaction ($\mathbf{C_B}$) is the strongest interaction in region 2 with an interaction energy of -2.83 kcal/mol calculated at CCSD(T)/CBS level (Figure S5, Supporting Information). It is noticeable that structure with S_2–S_1···S_3 angle of 90°, with non-bifurcated interaction ($\mathbf{C_{NB1}}$) is strong, $E_{CCSD(T)/CBS}$ = -2.55 kcal/mol (Figure 8). The second non-bifurcated interaction in $\mathbf{C_{NB2}}$ geometry is calculated to be $E_{CCSD(T)/CBS}$ = -1.66 kcal/mol.

Within regions 1 and 3 (Figure 5) for model system C (Figure 4), interaction energies are quite strong; -2.47 kcal/mol for $\mathbf{C_{NB3}}$ and -3.26 kcal/mol for $\mathbf{C_{NB4}}$ geometry (Figure 8). This energy is the strongest interaction energy for all studied model systems calculated (Tables 1, S6). In this geometry, S1–S2···S3 angle is 170°, and it possesses suitable electrostatic interaction of the two sulphur atoms, which makes this interaction very strong. Results of electrostatic potential maps calculations given at the end of this section will be used to explain the energy of the interactions.

In model system **D** (Figure 4) positive potential on the sulfur atom (*σ-hole*) of dimethyl sulfide is directed towards negative potential on the disulfide bond from another molecule. For model system **D**, non-bifurcated S_2–S_1···S_3 interaction energy ($\mathbf{D_{NB1}}$, Figure 9) is stronger than in corresponding $\mathbf{A_{NB1}}$ and $\mathbf{B_{NB1}}$ geometries but somewhat weaker than in $\mathbf{C_{NB1}}$, and is calculated to be $E_{CCSD(T)/CBS}$ = -1.98 kcal/mol.

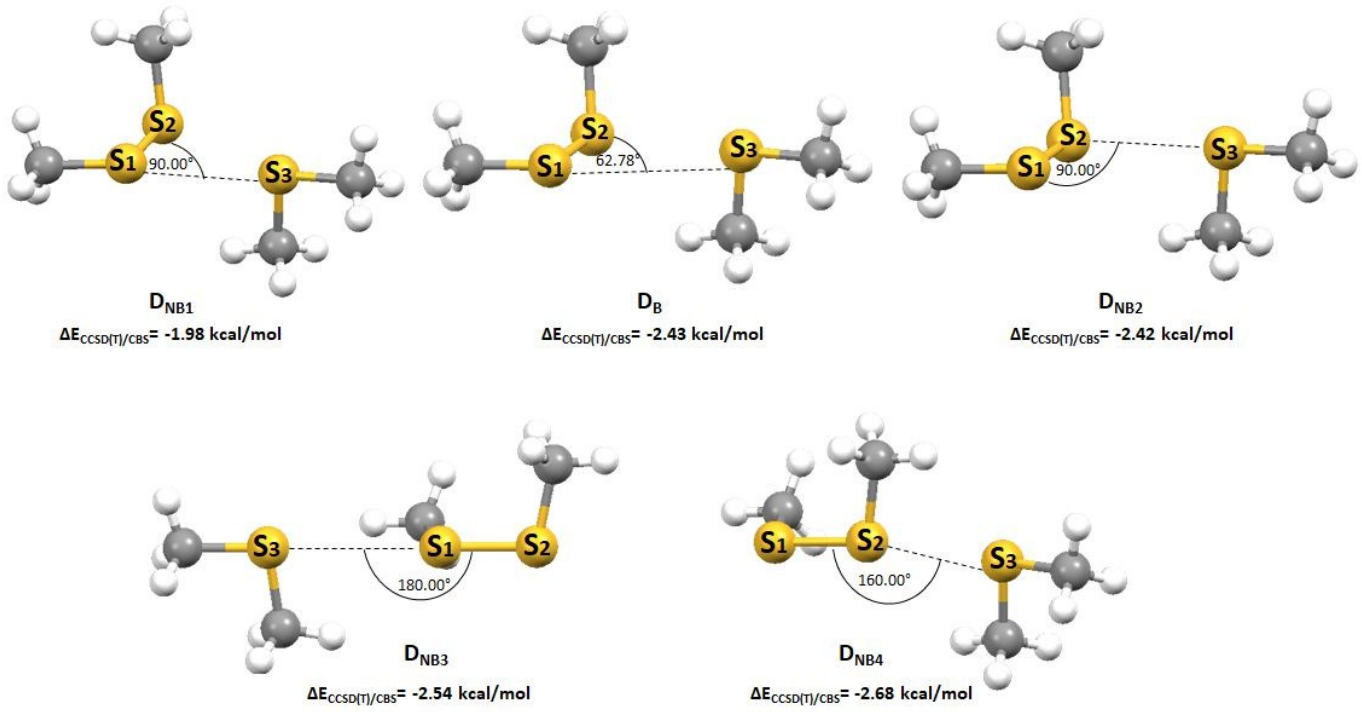

Figure 9. Geometries of four non-bifurcated (D_{NB1}, D_{NB2}, D_{NB3} and D_{NB4}) and bifurcated (D_B) interactions for model system D. Planes defined with atoms C–S_1–S_2 and C–S_3–C atoms are orthogonal.

View Article Online
DOI: 10.1039/D0CE00211A

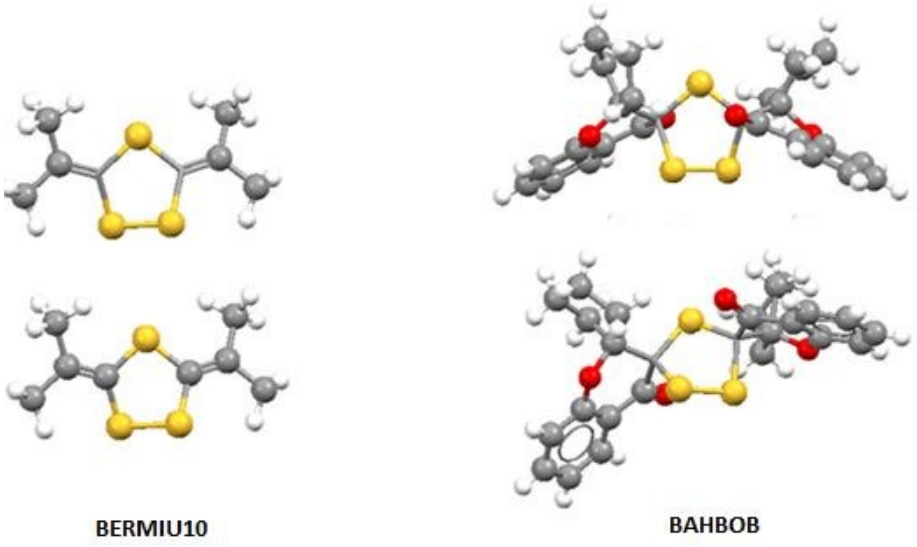

Figure 10. Examples of two crystal structures[50,51] containing substituents around disulfide bond that disable formation of S–S···S interactions with an angle of 180°. The CSD refcodes are given below each geometry.

As in the previous cases for model systems **A** and **C**, a bifurcated interaction is the strongest within the region 2. However, interaction energy of second non-bifurcated interaction for $\mathbf{D_{NB2}}$ geometry (Figure 9) is quite strong and almost the same as bifurcated one $\mathbf{D_B}$; -2.42 kcal/mol and -2.43 kcal/mol, respectively (Figure S6, Supporting Information). In comparison with non-bifurcated interaction in previous geometries, this interaction is significantly stronger.

Observing the interaction energies for model system D within regions 1 and 3 (Figure 5), we can notice that interactions in geometries around the sulfur atoms S_1 and S_2 are relatively strong (Figure 9, Table S6), similar to the model system **C**. This can be attributed to the formation of additional C–H···S interaction in those geometries.

Although the interactions are very strong in regions around S_1 and S_2 atoms (Tables 1, S6) in crystal structures there are no such geometries (Figures 2 and S4). Visual analysis of all crystal structures showed that this can be attributed to bulky substituents around disulfide bond (Figure 10). These substituents enclose the disulfide bond by stearic effect, thus formation of interactions with an angle of 180° is disabled.

The energy decomposition analysis

To further analyze the nature of S–S···S interactions, energy decomposition analysis was performed. The energy decomposition analysis was applied using SAPT 2+3 method and aug-cc-pVTZ basis set since the calculated total SAPT energies are in very good agreement with the CCSD(T)/CBS values (Table 1) which was shown in our previous study on S···S interactions and confirmed in this study.[16]

The SAPT calculations were performed on geometries presented in Figures 6–9. Results of SAPT analysis revealed that all geometries are stabilized by strong dispersion forces although electrostatic and induction energies are also attractive (Table 1). The largest attractive contribution to the total binding energy that originates from the dispersion energy term is similar to the previous results for the S···S interactions.[16] Although dispersion is the strongest, it is canceled by exchange component. Net-dispersion generally has very low values (both repulsive and attractive), except in geometries with very strong electrostatic component where net-dispersion is repulsive - over 1.0 kcal/mol (Table 1). Therefore, it is very important to emphasize influence of electrostatic component; the strongest interactions are those with the strongest electrostatics (see Figure S7, Supporting Information), so it can be concluded that electrostatics defines geometry of interaction. It is also important to note that in case of bifurcated interactions electrostatic and dispersion component is always stronger compared to non-bifurcated interactions while electrostatic component is stronger in most of the model systems.

Electrostatic Potential Maps

Since SAPT analysis indicates the importance of electrostatic component, we calculated electrostatic potential maps for both interacting molecules to more clearly explain studied geometries and their interaction energies.

As we mentioned previously, sulfur atoms can have a region of negative as well as a region of positive potential, enabling electrostatic attraction between two sulfur atoms.[15,16,25-27] In both molecules (dimethyl sulfide and dimethyl disulphide), the most positive potentials are on the hydrogen atoms (Figure 11, red color). The electrostatic potential map of dimethyl sulfide shows a negative region on the surface of the sulfur atom (Figure 11a, blue color) and in the direction of the S–CH_3 bond, a small area of positive potential (Figure 11a, yellow color).

If observed along the C-S_1-S_2 plane, the electrostatic potential map of dimethyl disulfide shows unequal distribution of charge on sulfur atoms along disulfide bond; a slightly negative region on the surface of one sulfur atom (Figure 11b, green color) and negative region on the surface of the other sulfur atom (Figure

View Article Online
DOI: 10.1039/D0CE00211A

ARTICLE

Table 1. Results of the SAPT Interaction Energy Decomposition and CCSD(T)/CBS Interaction Energies for Model Systems Given in Figures 6-9.

model system		$E_{electrostatic}$ (kcal/mol)	$E_{exchange}$ (kcal/mol)	$E_{induction}$ (kcal/mol)	$E_{dispersion}$ (kcal/mol)	$E_{"net\text{-}dispersion"}$ (kcal/mol)	$\Delta E_{SAPT2+3}$ (kcal/mol)	$\Delta E_{CCSD(T)/CBS}$ (kcal/mol)
A	$\mathbf{A_{NB1}}$	-0.889	3.843	-0.562	-3.598	0.245	-1.21	-1.20
	$\mathbf{A_B}$	-1.766	5.573	-0.797	-4.606	0.967	-1.60	-1.54
	$\mathbf{A_{NB2}}$	-0.076	1.910	-0.288	-2.255	-0.345	-0.71	-0.69
	$\mathbf{A_{NB3}}$	-0.790	3.008	-0.533	-3.218	-0.210	-1.53	-1.50
	$\mathbf{A_{NB4}}$	-1.951	3.970	-0.671	-3.267	0.703	-1.92	-1.88
B	$\mathbf{B_{NB1}}$	-0.101	2.591	-0.391	-2.860	-0.269	-0.76	-0.77
	$\mathbf{B_{NB2}}$	0.128	1.918	-0.296	-2.247	-0.329	-0.50	-0.49
C	$\mathbf{C_{NB1}}$	-3.127	7.156	-0.981	-5.648	1.508	-2.60	-2.55
	$\mathbf{C_B}$	-3.589	7.802	-1.028	-6.126	1.676	-2.94	-2.83
	$\mathbf{C_{NB2}}$	-1.141	3.529	-0.470	-3.662	-0.133	-1.74	-1.66
	$\mathbf{C_{NB3}}$	-2.259	5.513	-0.948	-4.836	0.677	-2.53	-2.47
	$\mathbf{C_{NB4}}$	-4.099	6.675	-1.107	-4.833	1.842	-3.36	-3.26
D	$\mathbf{D_{NB1}}$	-1.173	3.715	-0.558	-4.030	-0.315	-2.04	-1.98
	$\mathbf{D_B}$	-2.938	6.676	-0.976	-5.277	1.399	-2.51	-2.43
	$\mathbf{D_{NB2}}$	-3.063	6.696	-0.985	-5.142	1.554	-2.49	-2.42
	$\mathbf{D_{NB3}}$	-2.233	4.831	-0.804	-4.447	0.384	-2.65	-2.54
	$\mathbf{D_{NB4}}$	-2.278	4.411	-0.723	-4.171	0.240	-2.76	-2.68

11b, blue color). Region of positive electrostatic potential on sulfur atoms (*σ-hole*) could be observed in the direction of the S–S bond (Figure 11b, yellow and red color).

The difference between non-bifurcated S–S···S interactions in region 2 (Figure 5) for studied model systems can be explained by analysis of electrostatic potential maps (Figure 11). When $S_1 \cdots S_3$ non-bifurcated interaction is formed ($\mathbf{A_{NB1}}$, $\mathbf{B_{NB1}}$, and $\mathbf{C_{NB1}}$ geometries), negative region on sulfur atom from dimethyl sulfide (blue color, Figure 11a) is orientated towards slightly negative region on sulfur atom from dimethyl disulfide (green color, Figure 11b). When the $S_2 \cdots S_3$ non-bifurcated interaction is formed ($\mathbf{A_{NB2}}$, $\mathbf{B_{NB2}}$, and $\mathbf{C_{NB2}}$ geometries), very negatively charged region (blue color, Figure 11a) of one sulfur atom is orientated towards also very negatively charged region (blue color, Figure 11b) of the other sulfur atom which leads to weaker interactions.

The model system **D** (Figure 4) was made based on electrostatic potential maps, hence, positive potential on the sulfur atom (*σ-hole*) of dimethyl sulfide is in contact with the negative potential on the disulfide bond from another molecule. In this model system, second non-bifurcated $S_2 \cdots S_3$ interaction (-2.42 kcal/mol) is stronger than $S_1 \cdots S_3$ (-1.98 kcal/mol) since positive potential on the sulfur atom (*σ-hole*) from dimethyl sulfide is oriented towards very negative potential on the disulfide bond as mentioned before.

Interaction energies for the bifurcated geometries can also be explained by electrostatic potential maps since positive electrostatic potentials at the edges of hydrogen atoms (Figure 11a) can overlap with negative potential on disulfide bond (Figure 11b) which contributes to the strengthening of interaction.

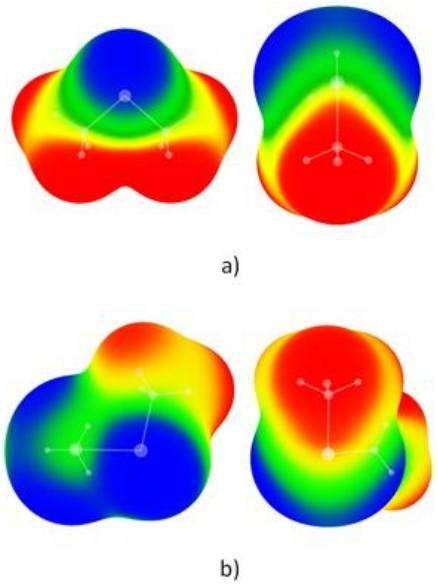

Figure 11. Computed MP2/cc-pVTZ electrostatic potentials on the 0.001 a.u. surface of a) dimethyl sulfide (two views) and b) dimethyl disulfide (two views). Color ranges, in kcal/mol, are: a) red, greater than 5.02; yellow, from 0.00 to 5.02 ; green, from -13.49 to 0.00; blue, more negative than -13.49; b) red, greater than 9.79; yellow, from 0.00 to 9.79 ; green, from -9.47 to 0.00; blue, more negative than -9.47.

In case of $\mathbf{A_{NB3}}$, $\mathbf{A_{NB4}}$, $\mathbf{C_{NB3}}$ and $\mathbf{C_{NB4}}$ geometries *σ-hole* of S_1 or S_2 atoms interact with negative potential on S_3 atom and make interaction very attractive. In geometries $\mathbf{D_{NB3}}$ and $\mathbf{D_{NB4}}$ positive (yellow and red color, Figure 11b) area around S_1 or S_2 atoms of dimethyl disulfide interacts with slightly negative (green color, Figure 11a) area around S_3 atom of dimethyl sulfide. These interactions are additionally strengthened by C-H···S hydrogen bonds.

Conclusions

In this paper, interactions between sulfur and disulfide bond have been systematically investigated by analyzing data from crystal structures archived in Cambridge Structural Database and by calculating their interaction energies using quantum chemical calculations. Results of statistical analyses of the crystal structures from CSD showed that bifurcated S–S···S interactions are widely present in crystal structures of small molecules and that small molecules have a tendency towards formation of bifurcated interactions rather than non-bifurcated. Relatively strong calculated S–S···S interaction is present in bifurcated geometry and the CCSD(T)/CBS energy of this interaction is -2.83 kcal/mol. Quite strong interaction energies are calculated for some non-bifurcated geometries. The strongest interaction energy found among studied model systems is -3.26 kcal/mol and is calculated for non-bifurcated S···S interaction accompanied with C-H···S hydrogen bond. The SAPT energy decomposition analysis showed that in bifurcated S–S···S interaction dispersion is the predominant attractive force, while contribution of electrostatic interaction is very significant. Analysis of electrostatic potential maps revealed that the strength of S–S···S interaction is related to the distribution of the positive and negative areas in the two molecules.

Results of quantum chemical calculations are in good agreement with the results of statistical analysis of crystal structure data and they lead to the same conclusion, that the bifurcated S–S···S interactions are stronger than non-bifurcated ones considering region along disulfide bond. Strong interactions calculated for non-bifurcated geometries are rare in crystal structures due to rigid and bulky substituents which sternly hinder the formation of such interactions in the supramolecular structure. These results could be of great importance in a variety of molecular systems containing sulfur atoms and disulfide bond, especially in biomolecules such as proteins.

Conflicts of interest

There are no conflicts to declare.

Acknowledgements

This work was supported by the Serbian Ministry of Education and Science (grant no. 172065). The HPC resources and services used in this work were partially provided by the IT Research Computing group in Texas A&M University at Qatar. IT Research Computing is funded by the Qatar Foundation for Education, Science and Community Development (http://www.qf.org.qa).

Notes and references

‡ Footnotes relating to the main text should appear here. These might include comments relevant to but not central to the matter under discussion, limited experimental and spectral data, and crystallographic data.

1 L. Junming, L. Yunxiang, Y. Subin and Z. Weiliang, *Struct. Chem*, 2011, **22**, 757–763.
2 R. E. Rosenfield Jr., R. Parthasarathy and J. D. Dunitz, *J. Am. Chem. Soc.*, 1977, **99**, 4860–4862.
3 T. N. Guru Row and R. Parthasarathy, *J. Am. Chem. Soc.*, 1981, **103**, 477–479.
4 G. R. Desiraju and V. Nalini, *J. Mater. Chem.*, 1991, **1**, 201–203.
5 R. Gleiter, D. B. Werz and B. J. Rausch, *Chem. - Eur. J.*, 2003, **9**, 2676–2683.
6 C. Bleiholder, R. Gleiter, D. B. Werz and H. Köppel, *Inorg. Chem.*, 2007, **46**, 2249–2260.
7 C. Bleiholder, D. B. Werz, H. Köppel and R. Gleiter, *J. Am. Chem. Soc.*, 2006, **128**, 2666–2674.
8 M. Iwaoka and N. Isozumi, *Molecules*, 2012, **17**, 7266–7283.
9 M. Iwaoka, S. Takemoto, M. Okada and S. Tomoda, *Chem. Lett.*, 2001, **30**, 132–133.
10 M. Iwaoka, S. Takemoto, M. Okada and S. Tomoda, *Bull. Chem. Soc. Jpn.*, 2002, **75**, 1611–1625.
11 M. Iwaoka, S. Takemoto and S. Tomoda, *J. Am. Chem. Soc.*, 2002, **124**, 10613–10620.
12 M. Iwaoka, in *Noncovalent Forces, Challenges and Advances in Computational Chemistry and Physics*, ed. S. Scheiner, Springer International Publishing, 2015, pp. 265–290.
13 E. W. Reinheimer, M. Fourmigue and K. R. Dunbar, *J. Chem. Crystallogr.*, 2009, **39**, 723–729.
14 R. Silaghi-Dumitrescu and A. Lupan, *Cent. Eur. J. Chem.*, 2013, **11**, 457–463.
15 P. Politzer, J. S. Murray and M. C. Concha, *J. Mol. Model.*, 2008, **14**, 659–665.
16 I. S. Antonijević, G. V. Janiić, M. K. Milčić and S. D. Zarić, *Cryst. Growth Des.*, **16**, 632–639.
17 (a) R. Shukla and D. Chopra, *Cryst. Growth Des.*, 2016, **16**, 6734–6742. (b) A. S. Mikherdov, A. S. Novikov, M. A. Kinzhalov, A. A. Zolotarev and V. P. Boyarskiy, *Crystals 2018*, **8**, 112, 1-15. (c) A. S. Mikherdov, A. S. Novikov, M. A. Kinzhalov, V. P. Boyarskiy, G. L. Starova, A. Yu. Ivanov and V. Yu. Kukushkin, *Inorg. Chem.*, 2018, **57**, 6, 3420-3433. (d) M. A. Kinzhalov, A. A. Eremina, D. M. Ivanov, A. S. Novikov, E. A. Katlenok, K. P. Balashev and V. V. Suslonov, *Z. Kristallogr. Cryst. Mater.* 2017, **232**, 797, 1-10. (e) A. S. Mikherdov, M. A. Kinzhalov, A. S. Novikov, V. P. Boyarskiy, I. A Boyarskaya, D. V. Dar'in, G. L. Starova and V. Yu. Kukushkin, *J. Am. Chem. Soc.* 2016, **138**, 42, 14129-14137.
18 J. Y. He, Z. W. Long and J. S. Zhang, *J. Struct. Chem*., 2011, **52**, 1057–1062.
19 M. Bai, S. P. Thomas, R. Kottokkaran, S. K. Nayak, P. C. Ramamurthy and T. N. Guru Row, *Cryst. Growth Des.*, 2014, **14**, 459–466.
20 J. M. Cole, C. M. Aherne, P. G. Waddell, A. J. Banister. A. S. Batsanov and J. A. K. Howard, *Polyhedron*, 2012, **45**, 61–70.
21 P. Hudhomme, S. Le Moustarder, C. Durand, N. Gallego-Planas, N. Mercier, P. Blanchard, E. Levillain, M. Allain, A. Gorgues and A. Riou, *Chem. - Eur. J.*, 2001, **7**, 5070–5083.

22 M. Mas-Torrent, P. Hadley, S. T. Bromley, X. Ribas, J. Tarres, M. Mas, E. Molins, J. Veciana and C. Rovira, *J. Am. Chem. Soc.*, 2004, **126**, 8546–8553.
23 X. Wang, W. Jiang, T. Chen, H. Yan, Z. Wang, L. Wan and D. Wang, *Chem. Commun.*, 2013, **49**, 1829–1831.
24 A. G. Flores-Huerta, A. Tkatchenko and M. Galván, *J. Phys. Chem. A*, 2016, **120**, 4223–4230.
25 J. S. Murray, P. Lane, T. Clark and P. Politzer, *J. Mol. Model.*, 2007, **13**, 1033–1038.
26 P. Politzer, J. S. Murray and T. Clark, *Phys. Chem. Chem. Phys.*, 2013, **15**, 11178–11189.
27 J. S. Murray, P. Lane and P. Politzer, *J. Mol. Model.*, 2009, **15**, 723–729.
28 (a) F. H. Allen, *Acta Crystallogr., Sect. B: Struct. Sci.*, 2002, **B58**, 380–388. (b) J. van de Streek, *Acta Crystallogr., Sect. B: Struct. Sci.*, 2006, **B62**, 567–579. (c) A. G. Orpen, *Acta Crystallogr., Sect. B: Struct. Sci.*, 2002, **B58**, 398–406. (d) F. H. Allen and W. D. S. Motherwell. *Acta Crystallogr., Sect. B: Struct. Sci.*, 2002, **B58**, 407–422. (e) R. Taylor. *Acta Crystallogr., Sect. D: Biol. Crystallogr.*, 2002, **D58**, 879–888.
29 Y. Zhang and W. Wang, *J. Mol. Struct.: THEOCHEM*, 2009, **916**, 135–138.
30 D. Ž. Veljković. G. V. Janjić and S. D. Zarić, *CrystEngComm*, 2011, **13**, 5005–5010.
31 J. Lj. Dragelj, G.V. Janjić, D. Ž. Veljković and S. D. Zarić, *CrystEngComm*, 2013, **15**, 10481–10489.
32 D. Ž. Veljković, V. B. Medaković, J. M. Andrić and S. D. Zarić, *CrystEngComm*, 2014, **16**, 10089–10096.
33 D. Ž. Veljković, *J. Mol. Graphics Modell.*, 2018, **80**, 121–125.
34 A. Bauzá and A. Frontera, *Molecules*, 2018, **23**, 699.
35 J. I. Bruno, C. J. Cole, R. P. Edgington, M. Kessler, F. C. Macrae, P. McCabe, J. Pearson and R. Taylor, *Acta Crystallogr., Sect. B: Struct. Sci.*, 2002, **B58**, 389–397.
36 M. J. Frisch, G. W. Trucks, H. B. Schlegel, G. E. Scuseria, M. A. Robb, J. R. Cheeseman, G. Scalmani, V. Barone, B. Mennucci, G. A. Petersson, H. Nakatsuji, M. Caricato, X. Li, H. P. Hratchian, A. F. Izmaylov, J. Bloino, G. Zheng, J. L. Sonnenberg, M. Hada, M. Ehara, K. Toyota, R. Fukuda, J. Hasegawa, M. Ishida, T. Nakajima, Y. Honda, O. Kitao, H. Nakai, T. Vreven, J. A. Montgomery, Jr., J. E. Peralta, F. Ogliaro, M. Bearpark, J. J. Heyd, E. Brothers, K. N. Kudin, V. N. Staroverov, R. Kobayashi, J. Normand, K. Raghavachari, A. Rendell, J. C. Burant, S. S. Iyengar, J. Tomasi, M. Cossi, N. Rega, J. M. Millam, M. Klene, J. E. Knox, J. B. Cross, V. Bakken, C. Adamo, J. Jaramillo, R. Gomperts, R. E. Stratmann, O. Yazyev, A. J. Austin, R. Cammi, C. Pomelli, J. W. Ochterski, R. L. Martin, K. Morokuma, V. G. Zakrzewski, G. A. Voth, P. Salvador, J. J. Dannenberg, S. Dapprich, A. D. Daniels, Ö. Farkas, J. B. Foresman, J. V. Ortiz, J. Cioslowski and D. J. Fox, Gaussian 09, Revision D.01, Gaussian, Inc., Wallingford, CT, 2013.
37 C. Møller and M. S. Plesset, *Phys. Rev,* 1934, **46**, 618–622.
38 R. A. Kendall, T. H. Dunning Jr. and R. J. Harrison, *J. Chem. Phys.*, 1992, **96**, 6796–6806.
39 D. E. Woon and T. H. Dunning Jr., *J. Chem. Phys.*, 1993, **98**, 1358–1371.
40 J. A. Pople, M. Head-Gordon and K. Raghavachari, *J. Chem. Phys.*, 1987, **87**, 5968–5975.
41 I. D. Mackie and G. A. DiLabio, *J. Chem. Phys.*, 2011, **135**, 134318.
42 S. F. Boys and F. Bernardi, *Mol. Phys.* 1970, **19**, 553–566.
43 B. Jeziorski, R. Moszynski and K. Szalewicz, *Chem. Rev.*, 1994, **94**, 1887–1930.
44 E. G. Hohenstein and C. D. Sherrill, *J. Chem. Phys.*, 2010, **133**, 014101.
45 R. M. Parrish, L. A. Burns, D. G. A. Smith, A. S. Simmonett, A. E. DePrince, E. G. Hohenstein, U. Bozkaya, A. Y. Sokolov, R. Di Remigio, R. M. Richard, J. F. Gonthier, A. M. James, H. R. McAlexander, A. Kumar, M. Saitow, X. Wang, B. P. Pritchard, P. Verma, H. F. Schaefer, K. Patkowski, R. A. King, E. F. Valeev, F. A. Evangelista, J. M. Turney, T. D. Crawford and C. D. Sherrill, *J. Chem. Theory Comput.*, 2017, **13**, 3185–3197.
46 R. F. W. Bader, M. T. Carroll, J. R. Cheeseman and C. Chang, *J. Am. Chem. Soc.*, 1987, **109**, 7968–7979.
47 F. A. Bulat, A. Toro-Labbe, T. Brinck, J. S. Murray and P. Politzer, *J. Mol. Model.*, 2010, **16**, 1679–1691.
48 A. Bondi, *J. Phys. Chem.*, 1964, **68**, 441–451.
49 M. Mantina, A. C. Chamberlin, R. Valero, C. J. Cramer and D. G. Truhlar, *J. Phys. Chem. A*, 2009, **113**, 5806–5812.
50 U. Kunze, R. Merkel and W.Winter, *Chem.Ber.*, 1982, **115**, 3653–3662.
51 F. A. G. El-Essawy, S. M. Yassin, I. A. El-Sakka, A. F. Khattab, I. Søtofte, J. Ø. Madsen and A. Senning, , *J.Org.Chem.*, 1998, **63**, 9840–9845.

Table of Contents

View Article Online
DOI: 10.1039/D0CE00211A

What is the preferred geometry of sulfur − disulfide interactions?

*Ivana S. Veljković, Dušan Ž. Veljković, Gordana G. Sarić, Ivana M. Stanković, Snežana D. Zarić**

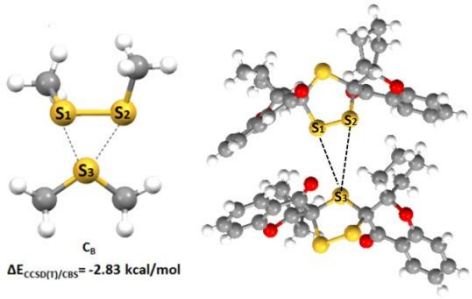

Combined crystallographic and quantum chemical study showed that in most cases in crystal structures interactions between sulphur atom and disulphide bond are bifurcated.